

END-TO-END FEL BEAM STABILITY SIMULATION ENGINE ^{*}

C. Serrano[†], L. R. Doolittle, LBNL, Berkeley, CA 94720, USA

D. S. Driver, A. F. Queiruga, B. Patel, Z. Zaky, University of California, Berkeley, CA 94720, USA

Q. Llimona, Universitat Pompeu Fabra, 08002, Barcelona, Spain

Abstract

During the design, commissioning and operation of a linac-driven Free Electron Laser (FEL) it is important to have a good understanding of the implications of accelerator design choices on beam figures of merit. This simulation engine combines a full state-space model of the RF system (High-Power Amplifier, RF cavities, LLRF controllers, etc.), a characterization of beam properties such as energy, bunch length and arrival time as electrons propagate through the Linac and beam-based feedback. The combination of these models with the ability to introduce both correlated and uncorrelated noise sources at any point of the machine, allows for a complete transposition of noise sources to beam performance parameters, including frequency dependence, in order to analyze implications of accelerator design choices in a simulation environment.

INTRODUCTION

New generation FELs like LCLS-II [1] (Light Coherent Light Source) permit not only the exploration of new fields of science, but the opportunity to generate ultra-stable beams. LCLS-II adds a 4 GeV L-band (1.3 GHz) superconducting linac operating in CW mode to the first 700 meters of the SLAC tunnel, increasing the repetition rate of LCLS from 120 Hz to 1 MHz. It allows for a dramatic increase of RF [2] and beam-based feedback [3] bandwidth and the associated benefits to beam stability.

A set of models were developed at Lawrence Berkeley National Laboratory (LBNL) during the preliminary studies of what is today LCLS-II. Based on LiTrack [4] and other models used for LLRF system studies [5] it was first implemented in Octave/Matlab, allowing an understanding of the basic physics concepts involved in the beam/feedback interactions [3]. The models have now been re-engineered and implemented with special care regarding computational efficiency and usability. On the functional level, support for cavity to cavity electro-mechanical interactions inside cryomodules has been introduced to assist in the design of the LCLS-II LLRF system [2].

OVERVIEW

Figure 2 shows the LCLS-II machine layout with all the components in the simulation engine. The models include beam instrumentation, considerations on latency in both the LLRF and beam-based feedback loops, as well as the ability to inject noise (both correlated and uncorrelated) at different points of the machine including a full characterization of the

electron gun performance parameters. The Linac is divided into generic building blocks composed of an accelerating section followed by a bunch compressor (where the bunch compressor can be enabled/disabled) and beam performance parameters are available after each one of these sections, which can then be used to apply beam-based feedback modulating RF set-points. Time-series data is computed at a configurable simulation step size and results can be visualized in both time and frequency domain, including transfer functions between any noise source and beam performance parameter to establish sensitivities numerically. Some of the newly implemented features are described next.

SOFTWARE ARCHITECTURE

The software architecture is layered to provide design modularity as shown in Figure 1. The back-end is implemented in computationally efficient C code and is wrapped using the Simplified Wrapper and Interface Generator (SWIG) to be called from other programming languages. In this implementation the simulation configuration is managed in Python and the C back-end is wrapped into a Python module using SWIG. The entire accelerator is described using JavaScript Object Notation (JSON) syntax and is parsed by the Python simulation program. The simulation program then allocates memory and resources for the back-end simulation engine based on the accelerator configuration and fills in the C data structures based on the configuration parameters.

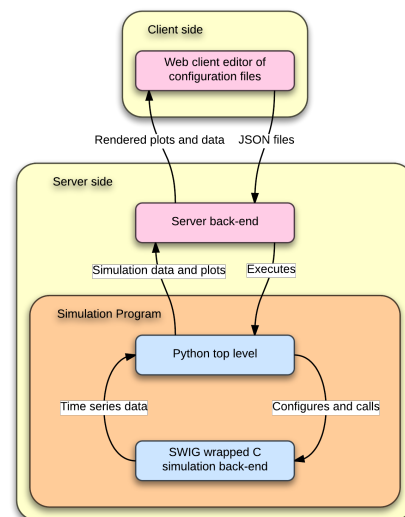


Figure 1: Software architecture.

^{*} Work supported by U.S. Department of Energy

[†] CSerrano@lbl.gov

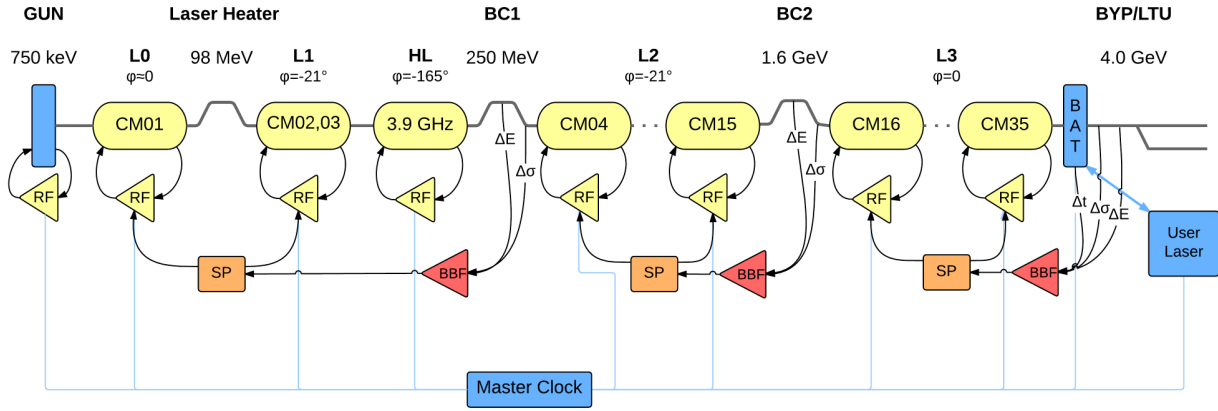


Figure 2: LCLS-II superconducting CW linac layout, featuring 35 1.3 GHz ILC-Tesla style cryomodules.

The simulator back-end is also modular so that any combination of accelerator components can be assembled for a simulation. This allows for high-level machine studies as well as lower level studies instantiating only a subset of the accelerator components.

The user interface is implemented in JavaScript. The user enters configuration parameters through a web browser and the client generates a JSON configuration file, which is sent to the web server. The server then calls the simulation program which parses the configuration files. They contain information about the layout of the simulation (how many linac sections, how many cryomodules per linac, cavities per cryomodule, etc.) and also the configuration parameters for each one of the entities instantiated (e.g. frequencies and Qs of RF cavities, loop latencies, beam phases, etc.). The simulation program allocates memory based on the layout, fills C data structures with the configuration parameters and calls the back-end simulation engine, receiving time-series data in return. The simulation data vectors can then be processed (e.g. FFT or transfer functions) in Python to provide plots for the server to send back to the user.

CAVITY MODEL

The cavity model responds to a multi-cell cavity structure, with couplings to the RF source, a cavity field probe and the beam. The cavity field is decomposed in its eigenmodes, where each mode is represented by the traditional RLC parallel circuit, coupled to two current sources representing the High Power Amplifier (HPA) and the beam respectively.

Ideally, we would like to measure the EM fields from each mode present in the cavity in order to control them appropriately. However, the best we can do is measure the overall field in the cavity, designated here by \vec{E}_{probe} . It is measured in practice using a probe antenna, and is theoretically given by

$$\vec{E}_{probe} = \sum_{\mu} \vec{V}_{\mu} / \sqrt{Q_{p\mu} (R/Q)_{\mu}} \quad (1)$$

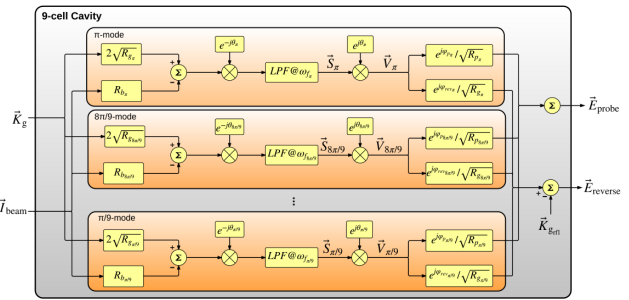


Figure 3: Software implementation of the cavity model.

where \vec{V}_{μ} is a representative measure of the energy stored in each electrical eigenmode μ , designated as mode cavity voltage, and where $Q_{p\mu} (R/Q)_{\mu}$ is the coupling impedance of the probe port for that mode.

Alternatively, the expression for reverse (a.k.a. reflected) wave traveling outward from the fundamental port includes a prompt reflection term, yielding

$$\vec{E}_{reverse} = \sum_{\mu} \vec{V}_{\mu} / \sqrt{Q_{g\mu} (R/Q)_{\mu}} - \vec{K}_g \quad (2)$$

where $Q_{g\mu} (R/Q)_{\mu}$ is the coupling impedance of the drive port of mode μ .

Equations 1 and 2 express the measured probe and reverse fields as a function of eigenmode voltages (\vec{V}_{μ}) and their respective port couplings, as illustrated in Figure 3. The state-variable equation governing the accelerating voltage for each eigenmode at baseband is given by

$$\left(1 - j \frac{\omega_{d\mu}}{\omega_{f\mu}}\right) \vec{V}_{\mu} + \frac{1}{\omega_{f\mu}} \frac{d\vec{V}_{\mu}}{dt} = 2\vec{K}_g \sqrt{R_{g\mu}} - R_{b\mu} \vec{I}_{beam} \quad (3)$$

where \vec{K}_g is the incident wave amplitude in $\sqrt{\text{Watts}}$, \vec{I}_{beam} is the beam current, and $R_{b\mu} = Q_{L\mu} (R/Q)_{\mu}$ is the coupling impedance to the beam. ω_f is the mode's bandwidth in rad/s and the $\frac{\omega_{d\mu}}{\omega_{f\mu}}$ term (the imaginary component of the mode's pole at baseband) represents detuning.

CRYOMODULE MODEL

Cryomodule elements (labeled *CM* in Figure 2) contain instantiations of a configurable amount of RF stations (RF cavity, controller, HPA, etc.) along with a model of the cryomodule's the mechanical resonances.

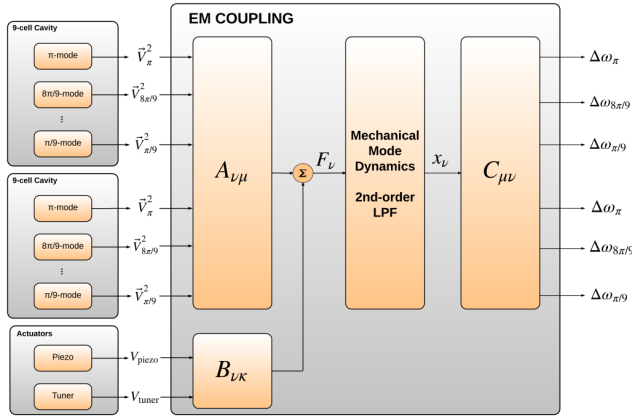


Figure 4: Software implementation of the cavity-to-cavity electro-mechanical interactions through Lorentz forces.

The presence of an EM field inside the cavity generates forces on the cavity walls, resulting in deformation of the cavity and subsequently in a shift of the cavity resonance frequency [6], designated as detune frequency $\omega_{d\mu}$. Each mode's fields generate a force proportional to $V_\mu^2 = |\vec{V}_\mu|^2$, and mechanical displacements influence each mode's instantaneous detune frequency. Construct ω_d as a baseline ω_{d0} from the electrical mode solution (e.g., $-2\pi(800 \text{ kHz})$ for the TTF cavity's $8\pi/9$ mode), plus a perturbation ω_μ contributed from the mechanical mode deflections,

Consider the electrical mode index μ to include not only electrical eigenmodes of one cavity, but modes of all cavities in the mechanical assembly (e.g., cryomodule). Also include the dependence on piezoelectric actuator voltages V_κ . Then if the assembly's mechanical eigenmodes are indexed by ν , mechanical forces F_ν and displacements x_ν of those eigenmodes are related to the electrical system by

$$F_\nu = \sum_\mu A_{\nu\mu} V_\mu^2 + \sum_\kappa B_{\nu\kappa} V_\kappa \quad (4)$$

$$\omega_\mu = \sum_\nu C_{\mu\nu} x_\nu \quad , \quad (5)$$

where A , B , and C are constant matrices. The software implementation of this calculation is illustrated in Figure 4.

MODEL INTEGRATION

Combining the Linac state-space models along with a model representing the longitudinal dynamics as the beam propagates through the Linac, we can calculate the effects of different noise sources in the system (both correlated and uncorrelated) on beam figures of merit such as energy stability, bunch length, peak current, timing stability, etc.

These quantities can be measured and used in order to apply corrections on the RF amplitude and phase set-points.

OPEN SOURCE

The implementation of the end-to-end simulation engine has been entirely written in various programming languages without the use of black boxes or proprietary software. The authors have been authorized by the U.S. Department of Energy to release the code to the public along with the documentation on the software and the physics involved. To fork the project visit the LBNL (*a.k.a.* Berkeley Lab) GitHub page [7].

CONCLUSION

A full end-to-end FEL beam stability simulation engine has been implemented using computationally efficient back-end code and supported by user friendly processing and visualization software. The simulation engine accurately represents the physics involved in the longitudinal beam dynamics as well as the interaction with the RF and beam-based feedback systems. It allows for the quantification of the effect of any noise source in the accelerator on the different beam figures of merit. The entire project, along with documentation of both the mathematical development of the models and the software implementation have been released by the U.S. Department of Energy to enable further collaborative efforts with the community.

REFERENCES

- [1] J. N. Galayda, "The new LCLS-II project: status and challenges," in *Proc. LINAC'14*, Geneva, Switzerland, August 2014, paper TUIOA04, pp. 404–408.
- [2] L. R. Doolittle *et al.*, "LLRF Control of high Q_L cavities for the LCLS-II," in *Proc. IPAC'16*, Busan, South Korea, May 2016, paper WEPOR042.
- [3] M. Mellado Munoz, L. Doolittle, P. Emma, G. Huang, A. Ratti, C. Serrano, J. M. Byrd, "A Dynamic feedback model for high repetition rate LINAC-Driver FELs," in *Proc. IPAC'12*, New Orleans, LA, May 2012, paper WEPPP073, pp. 2879–2881.
- [4] K.L.F. Bane, P. Emma, "LiTrack: A fast longitudinal phase space tracking code with graphical user interface," in *Proc. PAC'05*, Knoxville, TN, May 2005, pp. 4266–4268.
- [5] A. Vaccaro, L. Doolittle, A. Ratti, C. Serrano, "Hardware-Software Simulation for LLRF control system development," in *Proc. EPAC'08*, Genoa, Italy, June 2008, paper TUPC153, pp. 1428–1430.
- [6] J. R. Delayen, "Ponderomotive Instabilities and Microphonics – A Tutorial", in *Proc. SRF'05*, Ithaca, NY, July 2005, paper SUP01, pp. 35–39.
- [7] LBNL GitHub Page, <https://github.com/BerkeleyLab>